3-31-2016

The Impact of Damage Accumulation on the Kinetics of Network Strength Recovery for a Physical Polymer Gel Subjected to Shear Deformation

Travis Thornell

Krithika Subramaniam

Kendra Erk

The Impact of Damage Accumulation on the Kinetics of Network Strength Recovery for a Physical Polymer Gel Subjected to Shear Deformation

Travis L. Thornell, Krithika Subramaniam, Kendra A. Erk

School of Materials Engineering, 701 West Stadium Avenue, West Lafayette, IN, USA 47907-2045

Correspondence to: Kendra A. Erk (E-mail: *erk@purdue.edu*)

ABSTRACT

Shear rheophysical experiments were used to quantify the kinetics of strength recovery of model thermoreversible polymer gels that were fractured and ultimately sheared to different total magnitudes of strain (700 and 4000%) before resting for set periods of time. Relationships between the amount of strength recovered and the normalized ratio of resting times to characteristic relaxation times were developed. It was found that gels displayed fully healed networks within timescales that were 2-3 orders of magnitude greater than the gel's characteristic relaxation time. Gels deformed to 700% applied strain either healed slower at lower gel concentrations as compared to experiments at larger applied strains due to possible viscous heating or healed faster from incomplete fracture propagation for higher gel concentrations.

KEYWORDS: gels; kinetics; block copolymers

INTRODUCTION

A growing number of studies in the biomedical community are focused on the successful delivery of therapeutic drugs and cells for regenerative medicine applications.[1–3]A common route of delivery to the patient is through syringe injection. The high shear stresses present during injection would likely damage cells and disrupt viability.[4] However, by using a self-healing material as a carrier, it is believed that the cells can be better protected from external forces. These materials work to protect the cargo during injection by dissipating the force of the applied shear from the syringe and self-heal at the injection site to continue the release of the cells. Self-healing materials have been used as biomedical bone cements[5] to dental fillings[6] as well as self-healing coatings[7] and carbon fiber matrix composites.[8]

Polymer gels exhibiting a self-healing response are a suitable material class to use for injection delivery. Specifically, physical polymer gels could be particularly useful materials. These gels are composed of three-dimensional transient networks that have crosslinks formed via bonding from electrostatic, enthalpic or hydrogen bonding in response to environment (pH, temperature, etc.)[9] which differentiates them from chemical (covalent) crosslinked gels.[10] Gels that absorb water or biological fluids within the network are referred to as polymer hydrogels. Researchers have designed many different injectable hydrogels using pluronics[11], chitosan[12] and polymer-grafted nanoparticles.[13]

Many physical gels display self-healing behavior, but the kinetics and the governing timescales of network healing have not been fully investigated. Experiments quantifying the healing timescales of the networks are difficult to perform due to the viscoelastic nature of the gels. Viscoelastic gels are more difficult to characterize due to the relaxation of the viscous portion of their mechanical response. Conventional mechanical testing methods such as compression and tensile tests are more suitable for self-supporting

and high-modulus "tough" gels such as double network hydrogels[14,15], which do not relax significantly during the timescales of the measurement. These types of materials can be used for cartilage and tissue replacements.[16]

Several methods for characterizing the fracture-healing behavior of viscoelastic gels have been proposed in literature using shear rheological experiments.[13,17–20] These methods typically use oscillation based measurements to evaluate post-deformation strength recovery and are similar to the tests used to measure network gelation kinetics.[21,22] For "shear thinning" injectable materials, the material's storage modulus (G') is the critical parameter used to quantify self-healing behavior because it describes the elastic character of the material. These tests are performed in the following way. First, the material is deformed in rotation at very high shear rates (~100-1000 s^{-1}) causing the storage modulus to rapidly decrease. Second, by performing oscillatory measurements at constant frequency and small strain amplitude, G' is typically observed to increase over time to match its original value, which is thought to indicate full strength recovery or "healing" of the material.[17,23]

In our previous work, fracture-healing behavior was investigated by rotational constant shear rate experiments to probe fracture and shear banding of physically associating gels.[24] The shear stress response of the network was measured as a function of strain, and simultaneous flow visualization was performed to directly correlate the measured overshoots in the shear stress response with shear-induced strain localization taking place within the gels in the form of macroscale fracture planes and shear bands.

In more recent work, this rotational testing technique was adapted to quantify the ability and speed of the fractured gels to heal by halting the applied shear rate and allowing the gels to rest unperturbed for a set time before undergoing a second regime of applied shear.[25] This "shear-rest-shear" measurement protocol is different from the oscillatory techniques used by others[13,17–20], in which the gel was always exposed to some small amount of deformation during the period of recovery.The applied shear rate (1 s^{-1}) is also much lower than those used to shear thin materials discussed previously for the oscillation time sweeps.

In this article, we report the effects of damage accumulation on the fracture-healing kinetics of model acrylic triblock thermoreversible gels. A brief review and discussion of previous work will be presented. The remainder of the paper will investigate the effects of total strain duration on the gels. By investigating gels at near-fracture strains, the recovery timescales are hypothesized to decrease due to reduced damage accumulation.

EXPERIMENTAL

Materials

The model triblock gel from Kuraray Co. (Japan) consisted of poly(methyl methacrylate) (PMMA) end blocks of molecular weight of 8.9 kg/mol connected with a poly(n-butyl acrylate) (PnBA) midblock of 53 kg/mol. The polymer was dissolved in a midblock selective solvent, 2-ethyl hexanol (Sigma Aldrich, used as received), to form gels at concentrations of 5.0, 5.5, and 6.0 vol. %. Concentrations were selected to be above the critical micelle concentration of the solution and below the maximum torque limit of the rheometer.[26] Samples were prepared in scintillation vials and mixed at 80°C for 4 hours to form polymer solutions. Vials were then cooled to below a critical temperature of 34°C to form gels. For temperatures below 34°C, the network self assembles into PMMA endblock junctions connected by PnBA bridges.[26,27] The temperature-dependent nature of these gels is reflected in their characteristic relaxation times (τ_c) and small-strain (elastic) shear modulus values (G(0)) that are reported in Table 1[25] as temperature is

increased, the gels become mechanically weaker and more easily deformed (i.e., G decreases) and τ_c decreases significantly, indicating a shift to more viscous, liquid-like behavior in which any applied external stress would be quickly relaxed by the system.

Rheometry

Rotational shear rheometry experiments were conducted with an Anton Paar MCR 702 with a concentric cylinder fixture (CC27 cup-and-bob; gap=1 mm). The vial containing the sample (i.e., a gel at some set polymer concentration) was heated and the sample was poured into the fixture cup and cooled at a rate of 2°C/min to desired testing temperature (ranging from 28-20°C). The sample was allowed to equilibrate for 30 minutes. Figure 1 presents a visual representation of the "shear-rest-shear" measurement protocol, including some representative data. The protocol began by initiating a shear start-up test with constant shear rate ($\dot{\gamma}$) of 1 s^{-1} to the sample. The shear stress response was measured as a function of strain, and the observed stress overshoot was referred to as the sample's "primary fracture." Next, the sample was allowed to rest unperturbed in the rheometer for a set "resting time" (t). Then, the same shear rate was re-applied and a new stress overshoot was observed, referred to as the sample's "recovery fracture." The amount of strength recovered during the prescribed resting time was quantified by a ratio of stress maxima from the primary and recovery fracture responses (see Figure 1). Multiple tests were performed on each sample as the thermoreversible gel's mechanical history could be reset upon heating and cooling.

Particle Image Velocimetry

Following from our previous work, rheophysical measurements were used to directly correlate the shear-induced overshoots observed in a sample's stress response with the onset of cohesive (i.e., mid-gap) fracture taking place in the sample. To achieve this, rheometry measurements coupled with simultaneous particle image velocimetry[24,25,28] were performed with a custom-built assembly employing an Anton Paar MCR 302 shear rheometer with a transparent concentric cylinder fixture (Anton Paar CC32; gap = 1.5 mm). Temperature was controlled by a water bath and equilibrated for 30 minutes prior to testing. Details on the rheophysical instrumentation have been described previously[25,29] and are briefly summarized here. For particle tracking, samples are loaded with a 200 ppm concentration of 10-20 µm diameter silver-coated hollow glass microspheres. To illuminate the microspheres, a 405 nm wavelength laser (OBIS 405LX, Coherent) was guided into a laser sheet by concave and convex lenses and directed across the 1.5 mm gap of the transparent rheometer fixture (containing the sample). A CCD camera (dicam pro, pcoTech) with spatial resolution of 1280 x 1024 pixels and temporal resolution of 8 frames per second (fps) was appropriately positioned below the rheometer fixture to capture images of the plane of illuminated microspheres. For increased magnification, a Zoom 70XL lens (Qioptik) with basic bottom function module and 1.0X TV Tube was attached to the camera. A function generator and an oscilloscope were required to connect the rheometer and camera to take pictures at the required rate when experiments were started. Captured images were analyzed using PTVlab.[30] Previous work has shown no evidence of wall slip during testing of these gels.[24,25]

TABLE 1 Summary of the characteristic relaxation times (τ_c), and the small-strain shear modulus (G(0)) for 5-6 vol. % gels[25]

Concentration (vol%)	Characteristic Relaxation Times (τ_c)				Small-Strain Shear modulus (G(0))			
	28°C (sec)	25°C (sec)	23°C (sec)	20°C (sec)	28°C (Pa)	25°C (Pa)	23°C (Pa)	20°C (Pa)
5.0	2.4	10	50	120	90	140	180	250
5.5	2.5	15	40	130	180	260	310	400
6.0	3	20	30	120	300	410	470	540

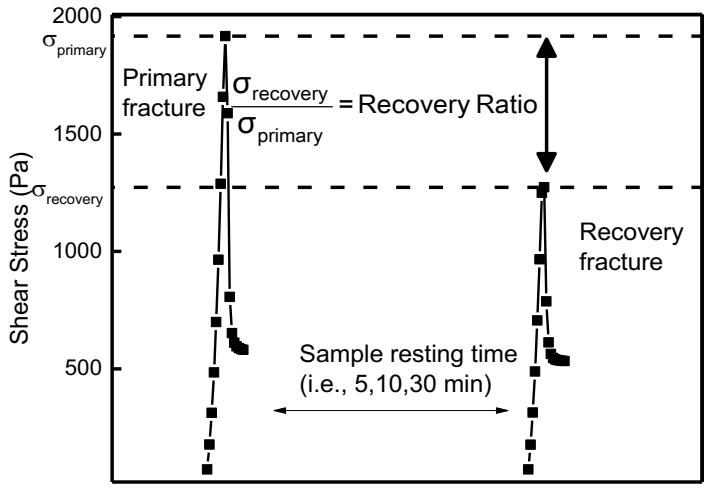

FIGURE 1. The "shear-rest-shear" measurement protocol, including representative shear stress versus time data for a 5.5 vol. % gel deformed at 23°C with a set resting time of 10 minutes.

RESULTS AND DISCUSSION

Relationship Between Gel Healing Kinetics and Characteristic Relaxation Behavior

In previous work[25], the fracture-healing behavior of the thermoreversible gels was studied using constant shear rate experiments over a total strain duration of 40 absolute units (4000% or γ_{40}) during the primary and recovery fracture tests separated by a set resting time that ranged from 5 minutes to several hours. By comparing the values of the stress overshoot maxima (recall Figure 1), the ratio of recovered strength was calculated; this ratio is reported as a percentage in Figure 2A for all gel concentrations and temperatures. Larger percentages indicated that during a given resting time, the gel was able to more completely heal and recover its mechanical strength, and longer resting times equated to greater percentages. This behavior is explained by the underlying fracture-healing mechanisms: the sharp stress relaxation indicated by the stress overshoot is due to the breakdown of the gel's self-assembled network structure by shear-induced removal of elastically active chains from their respective network junctions; and while the fractured gel is at rest, strength recovery or "healing" occurs when those dangling chains are able to re-associate into new network junctions and become elastically active again. The data also indicates that at each resting time, a wide range of stress recovery values were possible depending on the temperature of the system. For example, for relatively short resting times of 5 min, the stress recovered values ranged from 23% at 20°C to 99% at 28°C. Thus, increased temperature led to faster healing kinetics for all gel concentrations investigated here.

From Figure 2A, it is clear that the healing kinetics can be expressed as power law-type relationships for each temperature. In past work, time-temperature Arrhenius activation energy relationships were used to describe the healing kinetics. However, a more useful comparison to make is with the sample's characteristic relaxation time (τ_c). Figure 2B reports the same data as Figure 2A but now the resting times are normalized by the appropriate τ_c values from Table 1. The characteristic relaxation time values were determined from fitting a stretched exponential equation to relaxation modulus data obtained from step-strain experiments at different temperatures with a relatively small value of applied strain (5%, within the linear viscoelastic regime of the system).[26] For physical gels, including those studied here, τ_c can be thought of as the time required for the removal of elastically active molecules from their network junctions and subsequent relaxation of the stress within the molecule.[27]

As seen in Figure 2B, after normalization the data collapsed into an almost uniform trend described by a power law mathematical relationship. Table 2 summarizes the power law best fit equations for each gel concentration as well as the master curve, which is displayed in Figure 2B. From this analysis, we see that the time required for complete, 100% stress recovery of a fractured gel (referred to hereafter as the t_{100}) was on the order of 100-1000 times respective τ_c of the polymer networks. The t_{100} values for all samples investigated in this study are summarized in Table 3. Since healing was found to be dependent on resting time and system temperature, a fractured gel was able to fully heal if given sufficient rest, and healing was accelerated by increasing the temperature for the system.

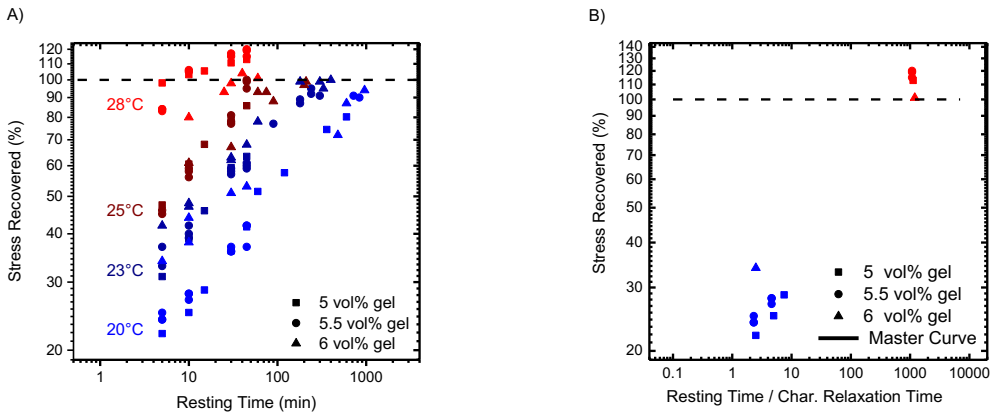

FIGURE 2 (A) Stress recovery as a function of resting time (t) for gels deformed at various concentrations and temperatures with the shear-rest-shear measurements protocol (γ_{40} data). (B) Data normalized by the characteristic relaxation times (τ_c) of the gel.

TABLE 2 Power law best fit parameters for $y=ax^b$ of γ_{40} data, where y=stress recovered as a percentage and x= t/τ_c, with a as the intercept and b as the exponent of healing.

Concentration (vol.%)	Intercept	Exponent of healing
5.0	19.92 ± 2.47	0.268 ± 0.025
5.5	21.50 ± 2.59	0.260 ± 0.024
6.0	30.03 ± 0.97	0.184 ± 0.005
Master Curve	23.09 ± 2.40	0.240 ± 0.020

Effect of Reduced Strain Duration on Healing Timescales

To more thoroughly investigate how the magnitude of the total applied strain in shear experiments may potentially influence the observed gel healing behavior, the shear-rest-shear measurement protocol was altered to reduce the total strain applied to samples during the "primary" and "recovery" constant shear rate experiments from 40 units of strain to only 7 units (illustrated in Figure 3). These different data sets will be referred to as γ_{4o} (already discussed in the last section, see Figure 2) and γ_7. The strain duration of 7 (700%) allowed for experiments to be completed near the decrease in shear stress response (i.e., the primary fracture of the gel). Figure 3 illustrates the difference in strain magnitude between γ_7 and γ_{4o} and the reproducibility of the shear stress maximum.

The effects of varying resting times on stress recovery can be seen in Figure 4 for a 5.5 vol. % gel tested at 23°C. Similar to γ_{4o} experiments analyzed in the past[25], the maximum of the stress overshoot (and thus the percentage of stress recovered) increased with resting time in the γ_7 experiments. For 10 min, only 40 % of the gel's initial strength was recovered, but recovery increased to 65 % after 30 min and 80 % after

45 min. Increasing the resting times to hours resulted in 90 % recovery after 1 hour, 95 % after 2 hours and > 99 % after 4 hours.

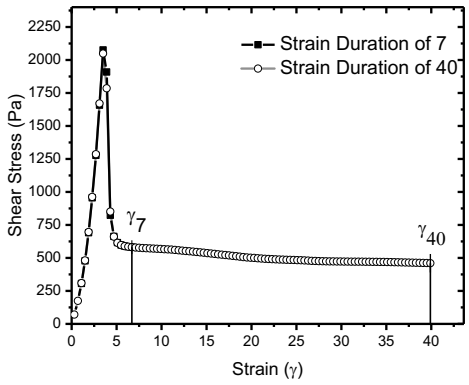

FIGURE 3. Stress responses during constant shear rate experiments for a 23 °C 5.5 vol. % gel, illustrating the difference in total strain duration for the γ_7 and γ_{4o} experiments.

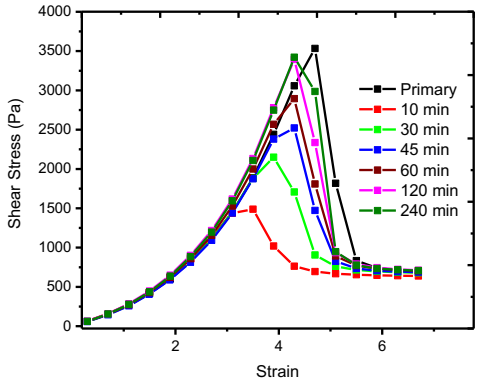

FIGURE 4. Primary and recovery fracture stress responses for γ_7 experiments of a 5.5 vol. % gel tested at 23 °C for various resting times.

Figure 5 reports the stress recovery of a 23°C, 5.5 vol. % gel following resting times of 5 to 258 min. At many values of resting time, a "high" and "low" value of stress recovered was observed; for examples, at 45 min, 83% and 71% stress recovery was found from shear-rest-shear experiments on the same sample. To analyze the spread in the data, power law and expanded power law fits were applied to (1) all data points (red curve in Figure 5), (2) the "high" data points (blue curve), and (3) the "low" data points (green curve). This created a range of t_{100} values for each sample when the fits were extrapolated to 100% stress recovered: for all data points, t_{100} was 189 mins; for high data points only, the value was 151 min; and for low data points only, t_{100} was 258 min. Overall, for the 5.5 vol. % gel deformed in γ_7 experiments at 23°C shown in Figure 5, the time required for 100% healing of the fractured network ranged from 151 min to 258 min. It is important to note that this extensive range of t_{100} values was not observed in γ_{4o} experiments. This "high-low" data analysis was performed for all γ_7 experiments and t_{100}

ranges are summarized in Table 3 in comparison with γ_{4o} experiments. Raw data and curve fits for gels at all concentrations and temperatures are reported in the online supporting information.

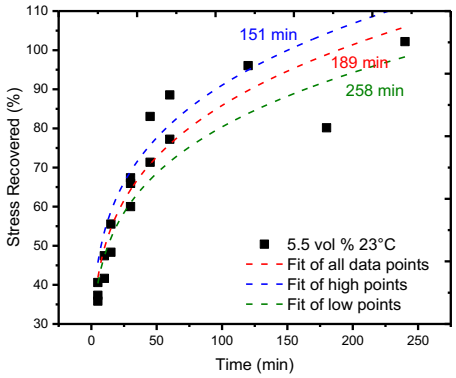

FIGURE 5. Percent of stress recovered versus time data for a 5.5 vol. % gel tested at 23°C with power law fits of high, low and all data points.

In a similar fashion to Figure 2A, stress recovery data normalized by τ_c for all γ_7 experiments are presented in Figure 6. The best fit lines from Table 2 for each gel concentration are added to Figure 6 in order to show the qualitative differences in the recovery behavior of γ_7 and γ_{4o} experiments. For 5 vol. % gels (Figure 6A), the "high-low" spread in the data points encompassed the γ_{4o} best fit line, indicating that the γ_7 experiments displayed both faster and slower healing kinetics. For 6 vol. % gels (Figure 6C), at most temperatures healing kinetics of the γ_7 experiments were faster than the γ_{4o} experiments. The 5.5 vol. % gels displayed intermediate behavior. Similar to the γ_{4o} experiments in Figure 2A, timescales for complete, 100% stress recovery (i.e., t_{100}) were again found to range from approximately (10^2-10^3) τ_c.

Directly comparing γ_7 to γ_{40} experiments summarized by Table 3 and Figure 6 indicated that as the gels were sheared to greater strain durations, the healing behavior was affected in a nonmonotonic way. Categorizing the results in terms of temperature and gel concentration, higher-temperature, lower-concentration samples deformed to greater strain (γ_{40}) displayed faster healing responses while lower-temperature, higher-concentration samples displayed faster healing for reduced strain durations (γ_7).

Our starting hypothesis in this study was that by investigating gels at near-fracture strains (i.e., with the γ_7 experiments), healing kinetics would be accelerated due to reduced total damage accumulation within the network as compared to experiments conducted at longer strain durations (i.e., the γ_{40} experiments) where greater total damage may occur, thus requiring more total time for 100% stress recovery. Instead, the data indicated that overall healing kinetics were similar in both cases if characteristic relaxation times were taken into account (i.e., $t_{100} \sim (10^2\text{-}10^3)\ \tau_c$), seemingly independent of the total amount of damage within the system. However, this simple analysis may be misleading, as the spread in the data from γ_7 experiments was found to be significantly greater than the corresponding γ_{40} experiments, with some samples displaying faster healing behavior and some slower. It may be that the observed "high-low" spread in γ_7 data was due to some samples displaying incomplete or "partial" fracture through the bulk (compared to total fracture through the gel). Intuitively, partial fracture may be more likely to occur for reduced strain duration experiments, where shearing was stopped immediately following the observed stress overshoot (recall Figure 3), potentially before the fracture plane was able to fully propagate through the bulk (note: the rheometer is expected to be sensitive to

even the onset of fracture in a gel, as explained in more detail in the next section). And such partial fracture may also heal more quickly, resulting in the rapid-recovery "high" data points that were frequently observed in γ_7 experiments.

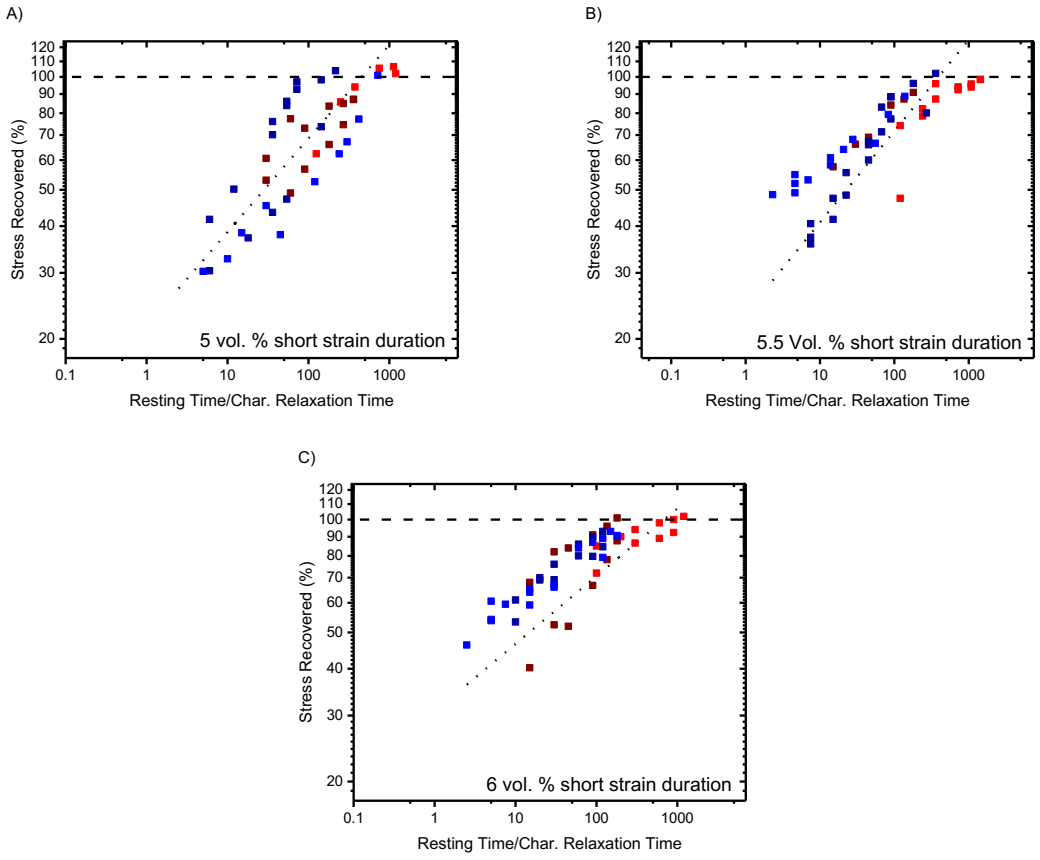

FIGURE 6. Stress recovery data from γ_7 experiments using the same formatting as Figure 2A for gel concentrations of (A) 5 vol. %, (B) 5.5 vol. % and (C) 6 vol. %. And temperatures from 20-28°C. Dotted lines are from the best fits reported in Table 2 from the γ_{40} data.

TABLE 3. Values of t_{100} (min) for fully healed networks determined from γ_7 and γ_{40} shear-rest-shear experiments; values from γ_7 experiments are in parenthesis.

Concentration (vol. %)		28°C (min)	25°C (min)	23°C (min)	20°C (min)
5.0	γ_{40}: γ_7:	3 (21-43)	40 (142-170)	150 (67-200)	700 (1060)
5.5	γ_{40}: γ_7:	11 (20-56)	50 (92)	350 (151-258)	1100 (934)
6.0	γ_{40}: γ_7:	25 (42-82)	210 (56-97)	400 (85-156)	1600 (556-921)

Investigation of Fracture with Rheophysical Experiments

Before further discussion of the likelihood of partial fracture in the γ_7 experiments, it is instructive to consider the rheophysical results. Velocity profiles from particle image velocimetry measurements of sheared gels have been measured previously and it was found that cohesive fracture occurred when these were deformed above a critical rate.[25] A linear velocity profile indicated deformation in a uniform manner-displaying simple shear with a single velocity gradient (i.e., one shear rate) existing between the moving wall to the stationary wall. When flow instabilities were present (such as fracture or shear banding), the velocity profiles became inhomogeneous and regions of different shear rates were formed. Evidence of midgap (cohesive) fracture events was observed when the velocity profiles were discontinuous, with regions of near-zero (or negative) velocity and regions of positive velocity of magnitude similar to the velocity of the moving wall. Following most fracture events, a region of negative local velocity was observed due to the elastic recoil of the gel moving in the opposite direction of the applied shear driven by the entropic elasticity of the polymer network.[31]

One of the main limitations of these and other similar rheophysical experiments[28] is that when only one laser-camera system is used, the velocity profile of only a relatively small area of the sheared sample can be investigated. Thus imaging of a flow instability in a system relies on the instability coming into the view of the camera (i.e., the small area of investigation). To verify the occurrence of fracture in our sheared gels (and correlate it with the occurrence of a stress overshoot in the rheometry data), experiments were typically extended to larger values of applied strain in order to ensure the complete propagation of fracture through the bulk system and into the view of our laser-camera assembly. This was always achieved for the γ_{40} experiments with the gels; however, for γ_7 experiments, these relatively "short" experiments successfully captured the stress overshoot (i.e., the onset of fracture in the gel), but discontinuous velocity profiles were not always directly observed due to potentially incomplete fracture propagation through the bulk of the gel.

Figure 7 illustrates the rheological data and velocity profiles of a 5.5 vol. % gel tested at 25°C. The stress overshoot shown in Figure 7A occurred at ~ 4 s (strain of 4 units). Using the laser-camera system to collect images of the illuminated tracer particles in the shear gel (every 0.2 s), Images 8-9 (strain of 2) have near-linear velocity, as expected for uniform simple shear behavior. For images 20-21 (strain of 4), where fracture was expected considering the occurrence of the stress overshoot in Figure 7A, instead linear velocity profiles were observed. The evidence of fracture did not appear until images 25-26 at 5.2 s (strain of 5). For these images, characteristic discontinuous velocity profiles were observed including negative values. This pronounced recoil was believed to impact the measured stress response of the gel shown in Figure 7A, a post-overshoot decrease and recovery in the data compared with the data in Figure 3. As the recoil response was a short-lived phenomenon, the stress response reaches its characteristic steady-state plateau after a few seconds. This delayed observation of fracture (i.e., expected in images 20-21 but not observed until images 25-26) most likely indicated the occurrence of incomplete fracture propagation through the gel; enough elastically active chains were pulled out of their respective junctions to impact the shear stress response, but fracture has not fully propagated through the entire polymer network and into the view of the laser-camera assembly.

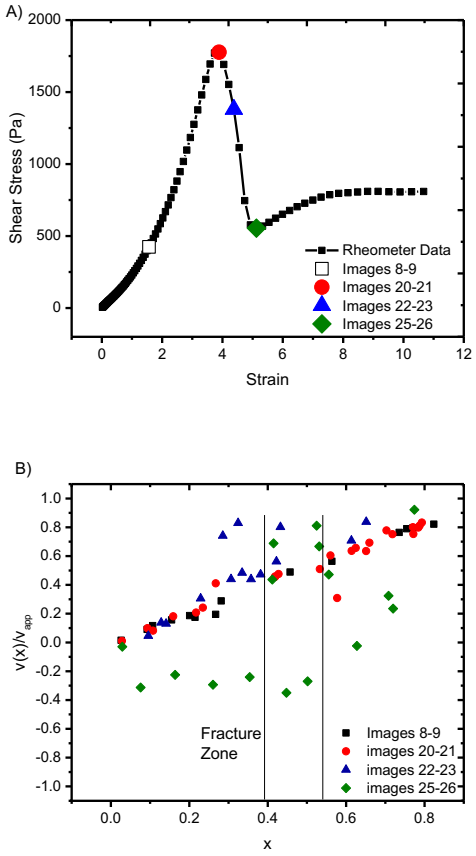

FIGURE 7. (A) Shear rheology data of a 25 °C, 5.5 vol. % gel during a constant shear rate test. (B) Calculated velocity profiles as function of relative distance across experimental gap for various images collected during rheophysical experiments. Vertical y-axis refers to the local velocity (v(x)) normalized with respect to the applied velocity, v_{app} (1.41 mm/s), and the horizontal x-axis (x) is the relative gap location within the experimental gap (1.5 mm), where x=0 is the location of the stationary wall of the cup and x=1 is the location of the moving wall of the rheometer fixture.

Effects of Network Structure and Properties on Healing Behavior

The 28°C data for the different experimental parameters indicated a change in the healing times of the gel. For the y_{40} experiments, gels quickly healed and were able, in some cases, to exceed the maximum strength of the primary fracture response. As the strain duration was decreased in y_7 experiments, the time for gels to heal at 28°C increased. The accelerated kinetics of the y_{40} experiments were believed to be due to local viscous heating within the sheared gel in the vicinity of the fracture zone.[32] With its critical temperature of 34°C, the gel was a relatively weak and highly transient network at 28°C. By having the rheometer fixture at the fixed gap of 1 mm rotating at the constant applied shear rate to a total strain of 40 units, the friction[24] within the fracture zone could lead to local increases in temperature by 1 or 2 °C. Once the experiment is halted, the thermal energy could disperse evenly through the sample to eliminate any temperature gradients. This localized heating could cause the network to become very dynamic and

act more similar to a polymer solution. Testing the gels at shorter times and lower total strain duration, as with the γ_7 experiments, would effectively minimize the effects of friction-induced heating.

Aggregation number and junction size could also influence the healing mechanism and timescales. Previously reported small-angle x-ray scattering (SAXS) data on gel concentrations above 10 vol. %[27] showed that aggregation number increased from 60 to 80 chains per junction for increasing concentrations from 10 to 30 vol. %. SAXS results for lower concentration gels were unobtainable due to weak scattering though based on the experimental trends, it is likely that the aggregation number was 40-50 chains per junction in the static (unsheared) state for the gel concentrations investigated here of 5-6 vol. %. It is unclear from experiments exactly how the "dangling", unassociated polymer chains reform into elastically active network strands during the resting period following shear-induced fracture; healing could occur by either dangling chains re-inserting into their original junction or perhaps forming new junctions of different size.

Simulations of telechelic polymers[33–35] that exhibit shear banding flow instabilities have shown that aggregation number can change during deformation. This could be due to the creation of dangling chains that are unable to reinsert into endgroup junctions. During high shear rates, more junctions are formed containing endblocks from the same polymer, forming loops and causing a range of junction sizes to be observed. From simulated oscillatory measurements, restructured networks with increased number of junctions were found to be stronger than the initial network. Small frequency oscillations of the system caused dangling chains to re-enter into existing junctions. Applying these conclusions to our work, a range of junction sizes could accelerate healing kinetics following shear-induced fracture and regain its strength by allowing dangling chains from fractured junctions to reinsert themselves into an existing junction.

Strength of the gel was dependent on temperature as described in Figure 8. As temperature decreased, the gel became more elastic and strain stiffen.[26] For the highest temperature of this study, 28°C, the gel was near the critical temperature and the network was more viscous and dynamic. As the temperature was decreased, the network becomes more rigid and the endblock junctions were more tightly packed as the increasingly poor solvent was expelled from the PMMA endblocks.[36] The stiffer network structure exhibited higher shear stress maxima.

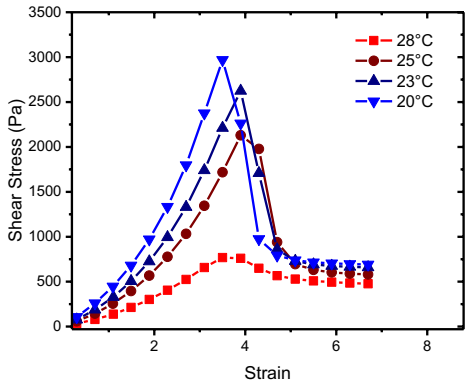

FIGURE 8. Stress-strain curves of 5.5 vol. % gels at various temperatures ranging from 28-20°C.

The temperature dependence of network strength can also be seen from the G(0) values in Table 1. Gel strength increased with increasing concentration and decreasing temperature, and there exists a general correlation between t_{100} and G(0) values. For gels with G(0) < ~300 Pa (i.e., 5 vol. % gels at all temperatures

and high temperature tests of 5.5 vol. % gels), t_{100} values from the y_{40} experiments were found to be smaller than t_{100} values from the y_7 experiments due to possible viscous heating of the system. As illustrated and described earlier in Figure 6A and 6B, stress recovery data displayed a "high-low" spread of healing behaviors for y_7 experiments, believed to be due to some systems only partially fracturing when exposed to these relatively shorter applied strain durations and able to then display accelerated healing. Interestingly, reduced t_{100} values of y_7 experiments were observed when G(0) > 300 Pa (i.e., gels at lower temperatures of 5.5 vol. % and 6 vol. %). This may indicate that partial fracture of the stiffer gels may lead to faster healing of the gels.

CONCLUSIONS

We have investigated the effect of deformation magnitude on the fracture-healing kinetics of model acrylic triblock copolymer gels at various concentrations (5-6 vol. %) and temperatures (20-28°C) using shear rheophysical experiments. By changing the total strain applied to the system (700 vs. 4000% applied strain) and varying the post-fracture resting times, variations in the strength recovery of the gels were measured.

- A gel can fully heal given sufficient post-fracture resting time, and healing kinetics can be accelerated by increasing the temperature of the system.
- Complete, post-fracture strength recovery occurred within timescales that were 2-3 orders of magnitude greater than the characteristic relaxation times of the gels.
- For 5 vol. % gels tested at all temperatures and 5.5 and 6 vol. % gels tested at high temperatures, healing kinetics were believed to be accelerated by local viscous heating within the system during the 4000% applied strain experiments.
- For the 700% applied strain experiments, 5.5 vol. % gels tested at lower temperatures and 6 vol. % tested at all temperatures required relatively shorter resting times to obtain a completely healed network due to the probable occurrence of partial or incomplete fracture propagation.
- Rheophysical experiments indicated a delay in visual observation of complete fracture following the measured stress overshoot, and this delay was more likely for 700% applied strain experiments, providing further evidence of partial fracture.

ACKNOWLEDGEMENTS

Authors would like to thank Kuraray Co. of Japan for the model triblock polymers. This work has been supported under a National Science Foundation Graduate Research Fellowship (DGE-1333468).

REFERENCES AND NOTES

1 H. Naderi, M. M. Matin and A. R. Bahrami, *J. Biomater. Appl.*, 2011, **26**, 383–417.

2 V. Gujrati, S. Kim, S. H. Kim, J. J. Min, H. E. Choy, S. C. Kim and S. Jon, *ACS Nano*, 2014, **8**, 1525–1537.

3 A. H. Van Hove, M.-J. G. Beltejar and D. S. W. Benoit, *Biomaterials*, 2014, **35**, 9719–9730.

4 B. A. Aguado, W. Mulyasasmita, J. Su, K. J. Lampe and S. C. Heilshorn, *Tissue Eng. Part A*, 2012, **18**, 806–815.

5 A. B. W. Brochu, W. J. Chyan and W. M. Reichert, *J. Biomed. Mater. Res. Part B Appl. Biomater.*, 2012, **100B**, 1764–1772.

6 B. E. Wertzberger, J. T. Steere, R. M. Pfeifer, M. A. Nensel, M. A. Latta and S. M. Gross, *J. Appl. Polym. Sci.*, 2010, **118**, 428–434.

7 G. Scheltjens, M. M. Diaz, J. Brancart, G. Van Assche and B. Van Mele, *React. Funct. Polym.*, 2013, **73**, 413–420.

8 K. R. Hart, N. R. Sottos and S. R. White, *Polymer* , 2015, **67**, 174–184.

9 S. Ahn, R. M. Kasi, S.-C. Kim, N. Sharma and Y. Zhou, *Soft Matter*, 2008, **4**, 1151.

10 M. Patenaude, N. M. B. Smeets and T. Hoare, *Macromol. Rapid Commun.*, 2014, **35**, 598–617.

11 Y. Lee, H. J. Chung, S. Yeo, C.-H. Ahn, H. Lee, P. B. Messersmith and T. G. Park, *Soft Matter*, 2010, **6**, 977.

12 Y.-L. Chiu, S.-C. Chen, C.-J. Su, C.-W. Hsiao, Y.-M. Chen, H.-L. Chen and H.-W. Sung, *Biomaterials*, 2009, **30**, 4877–4888.

13 E. A. Appel, M. W. Tibbitt, M. J. Webber, B. A. Mattix, O. Veiseh and R. Langer, *Nat. Commun.*, 2015, **6**, 6295.

14 R. Long, K. Mayumi, C. Creton, T. Narita and C. Hui, *Macromolecules*, 2014, **47**, 7243–7250.

15 T. L. Sun, T. Kurokawa, S. Kuroda, A. Bin Ihsan, T. Akasaki, K. Sato, M. A. Haque, T. Nakajima and J. P. Gong, *Nat. Mater.*, 2013, **12**, 932–937.

16 J. P. Gong, Y. Katsuyama, T. Kurokawa and Y. Osada, *Adv. Mater.*, 2003, **15**, 1155–1158.

17 S. Sathaye, A. Mbi, C. Sonmez, Y. Chen, D. L. Blair, J. P. Schneider and D. J. Pochan, *Wiley Interdiscip. Rev. Nanomedicine Nanobiotechnology*, 2015, **7**, 34–68.

18 T. Rossow, A. Habicht and S. Seiffert, *Macromolecules*, 2014, **47**, 6473–6482.

19 P. J. Skrzeszewska, J. Sprakel, F. A. de Wolf, R. Fokkink, M. A. Cohen Stuart and J. van der Gucht, *Macromolecules*, 2010, **43**, 3542–3548.

20 M. Gerth, M. Bohdan, R. Fokkink, I. Voets, J. van der Gucht and J. Sprakel, *Macromol. Rapid Commun.*, 2014, **35**, 2065–2070.

21 V. Normand, S. Muller, J. C. Ravey and A. Parker, *Macromolecules*, 2000, **33**, 1063–1071.

22 A. S. Sarvestani, X. He and E. Jabbari, *Biomacromolecules*, 2007, **8**, 406–415.

23 C. Yan, A. Altunbas, T. Yucel, R. P. Nagarkar, J. P. Schneider and D. J. Pochan, *Soft Matter*, 2010, **6**, 5143–5156.

24 K. A. Erk, J. D. Martin, Y. T. Hu and K. R. Shull, *Langmuir*, 2012, **28**, 4472–8.

25 T. L. Thornell, B. A. Helfrecht, S. A. Mullen, A. Bawiskar and K. A. Erk, *ACS Macro Lett.*, 2014, **3**, 1069–1073.

26 K. A. Erk and K. R. Shull, *Macromolecules*, 2011, **44**, 932–939.

27 M. E. Seitz, W. R. Burghardt, K. T. Faber and K. R. Shull, *Macromolecules*, 2007, **40**, 1218–1226.

28 Y. T. Hu and A. Lips, *J. Rheol.* , 2005, **49**, 1001.

29 A. Bawiskar, Purdue University, 2014.

30 W. Brevis, Y. Niño and G. H. Jirka, *Exp. Fluids*, 2011, **50**, 135–147.

31 M. Rubinstein and R. H. Colby, *Polymer physics*, Oxford University Press, 2003.

32 J. M. White and S. J. Muller, *J. Rheol.* , 2003, **47**, 1467.

33 J. Billen, M. Wilson and A. R. C. Baljon, *Chem. Phys.*, 2015, **446**, 7–12.

34 M. Wilson, A. Rabinovitch and A. R. C. Baljon, *Macromolecules*, 2015, **48**, 6313–6320.

35 S. Li, J. Chen, D. Xu and T. Shi, *J. Chem. Phys.*, 2015, **143**, 244902.

36 P. L. Drzal and K. R. Shull, *Macromolecules*, 2003, **36**, 2000–2008.

GRAPHICAL ABSTRACT

Travis L. Thornell, Krithika Subramaniam, Kendra A. Erk

The Impact of Damage Accumulation on the Kinetics of Network Strength Recovery for a Physical Polymer Gel Subjected to Shear Deformation

The fracture-healing behavior of model acrylic triblock copolymer gels was investigated with shear rheophysical experiments. The effect of deformation magnitude (700 vs. 4000% total applied strain) was studied to determine how damage accumulation may impact healing timescales. Fractured gels that were tested at relatively small strain durations typically healed faster than gels deformed to larger applied strains. Incomplete fracture propagation throughout the sample was possible for the reduced strain experiments as indicated by flow visualization.

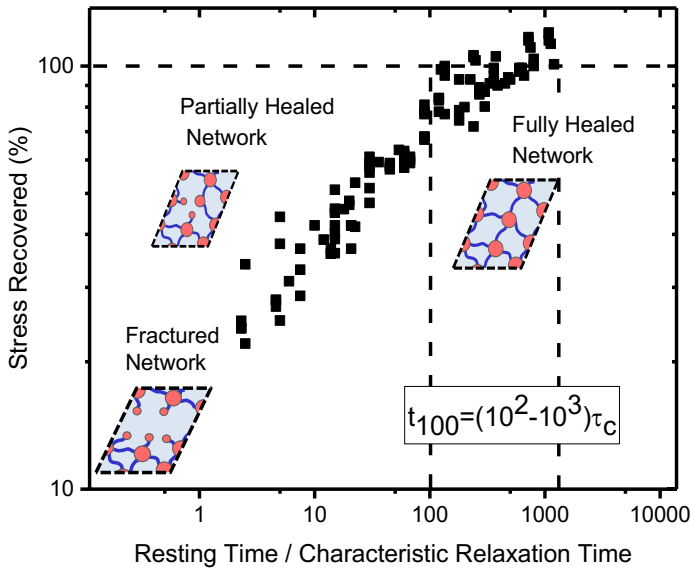

Supporting information for

The Impact of Damage Accumulation on the Kinetics of Network Strength Recovery for a Physical Polymer Gel Subjected to Shear Deformation

Travis L. Thornell, Krithika Subramaniam, Kendra A. Erk

School of Materials Engineering, 701 West Stadium Avenue, West Lafayette, IN, USA 47907-2045

% Recovery as a function of time for all concentrations and temperatures.

Fracture gels at γ_7 strains displayed "high and low" stress recovery. To better understand the effects of this on the time needed for 100 % stress recovery (t_{100}), power law type fits were applied to the range of collected data to gather information for all points, "high" points, and "low" points. Figures S1-S12 illustrate the raw data for all concentrations and temperatures with the applicable 3 fits and Tables S1-S12 summarize the fitting equations and t_{100}.

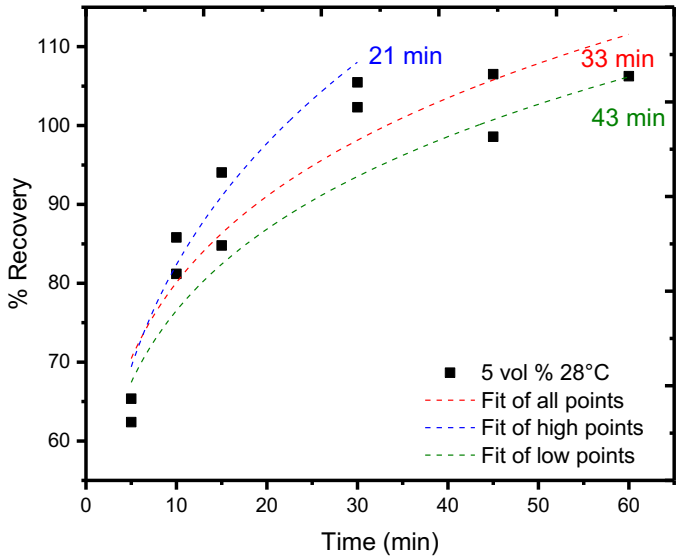

Figure S9. Recovery versus time data for 5 vol. % 28°C with power law fits of all, high, and low data points.

Table S1. Power law fits of 5 vol. % 28°C from Figure S1

Data Type	Equation	Healing Time (min)
Overall, all data	$Y=52.30x^{0.185}$	33
High Points	$Y=46.63x^{0.247}$	21
Low Points	$Y=50.25x^{0.193}$	43

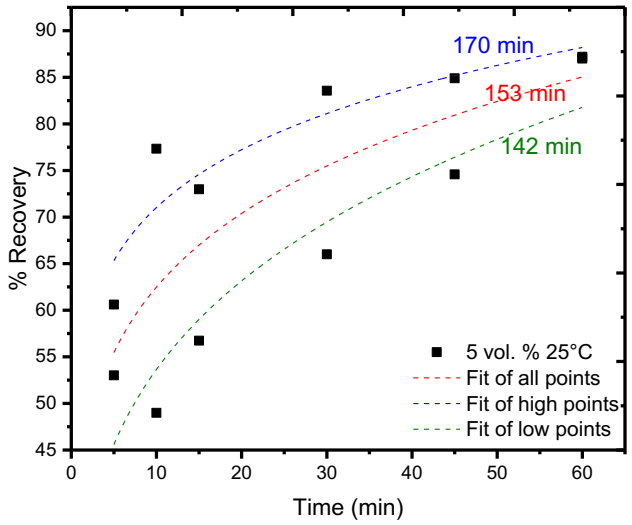

Figure S10. Recovery versus time data for 5 vol. % 25°C with power law fits of all, high, and low data points.

Table 2. Power law fits of 5 vol. % 25°C from Figure S2.

Data Type	Equation	Healing Time (min)
Overall, all data	$Y=42.04x^{0.172}$	153
High Points	$Y=53.78x^{0.121}$	170
Low Points	$Y=31.22x^{0.235}$	142

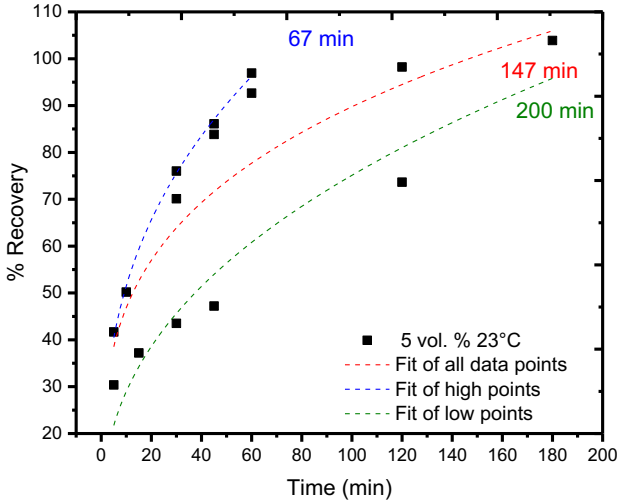

Figure S11. Recovery versus time data for 5 vol. % 23°C with power law fits of all, high, and low data points.

Table S3. Power law fits of 5 vol. % 23°C from Figure S3.

Data Type	Equation	Healing Time (min)
Overall, all data	$Y=24.46x^{0.282}$	147
High Points	$Y=23.07x^{0.349}$	67
Low Points	$Y=11.16x^{0.414}$	200

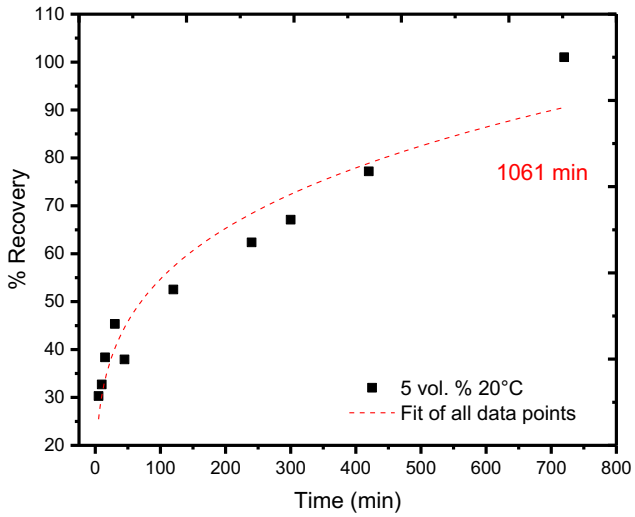

Figure S12. Recovery versus time data for 5 vol. % 20°C with power law fits of all, high, and low data points.

Table S4. Power law fits of 5 vol. % 20°C from Figure S4.

Data Type	Equation	Healing Time (min)
Overall, all data	$Y=16.87x^{0.255}$	1061
High Points	N/a	N/a
Low Points	N/a	N/a

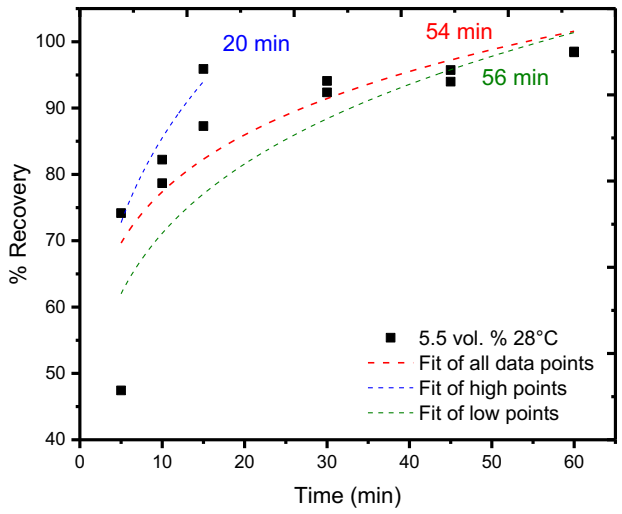

Figure S13. Recovery versus time data for 5.5 vol. % 28°C with power law fits of all, high, and low data points.

Table S5. Power law fits of 5.5 vol. % 28°C from Figure S5.

Data Type	Equation	Healing Time (min)
Overall, all data	$Y=54.55x^{0.152}$	54
High Points	$Y=49.94x^{0.234}$	20
Low Points	$Y=45.09x^{0.198}$	56

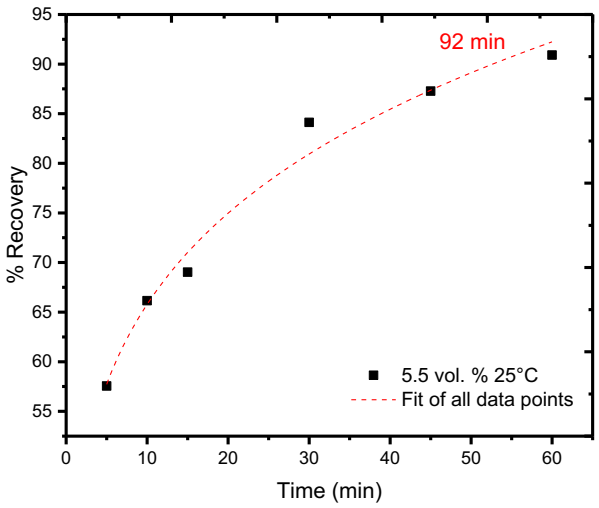

Figure S14 Recovery versus time data for 5.5 vol. % 25°C with power law fits of all, high, and low data points.

Table S6. Power law fits of 5.5 vol. % 25°C from Figure S6.

Data Type	Equation	Healing Time (min)
Overall, all data	$Y=42.60x^{0.189}$	92
High Points	N/a	N/a
Low Points	N/a	N/a

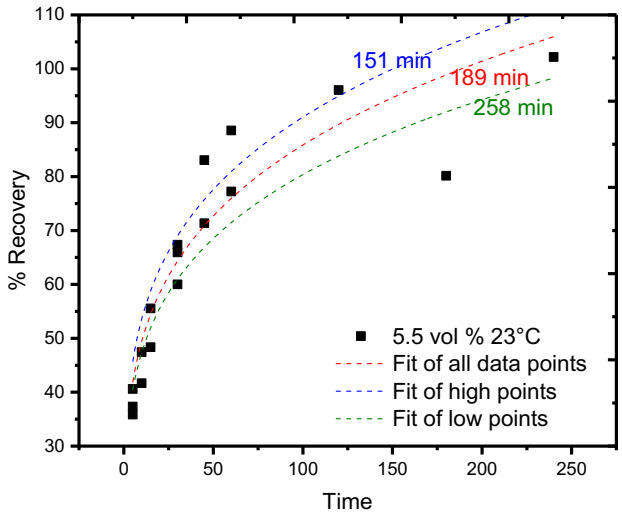

Figure S15 Recovery versus time data for 5.5 vol. % 23°C with power law fits of all, high, and low data points.

Table S7. Power law fits of 5.5 vol. % 23°C from Figure S7.

Data Type	Equation	Healing Time (min)
Overall, all data	$Y=28.44x^{0.240}$	189
High Points	$Y=31.52x^{0.230}$	151
Low Points	$Y=27.88x^{0.230}$	258

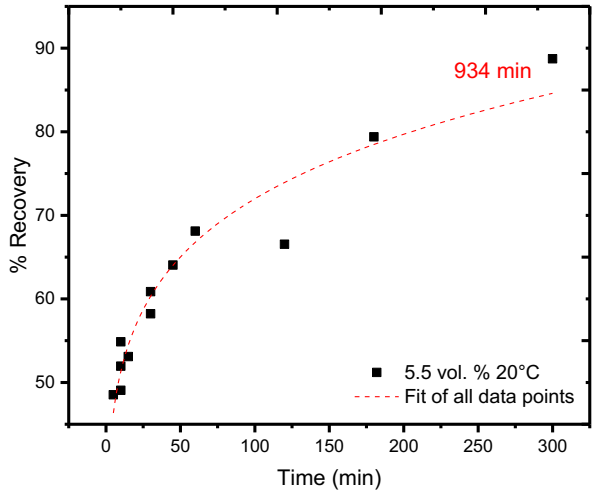

Figure S16 Recovery versus time data for 5.5 vol. % 20°C with power law fits of all, high, and low data points.

Table S8. Power law fits of 5.5 vol. % 20°C from Figure S8.

Data Type	Equation	Healing Time (min)
Overall, all data	$Y=36.58x^{0.147}$	934
High Points	N/a	N/a
Low Points	N/a	N/a

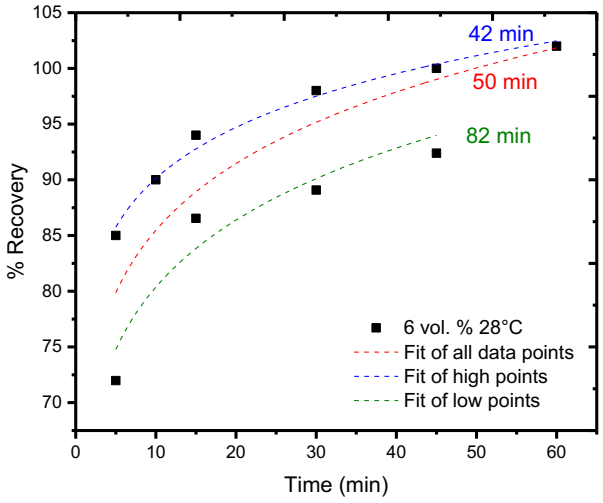

Figure S17 Recovery versus time data for 6 vol. % 28°C with power law fits of all, high, and low data points.

Table S9. Power law fits of 6 vol. % 28°C from Figure S9.

Data Type	Equation	Healing Time (min)
Overall, all data	$Y=68.23x^{0.098}$	50
High Points	$Y=76.41x^{0.072}$	42
Low Points	$Y=63.25x^{0.104}$	82

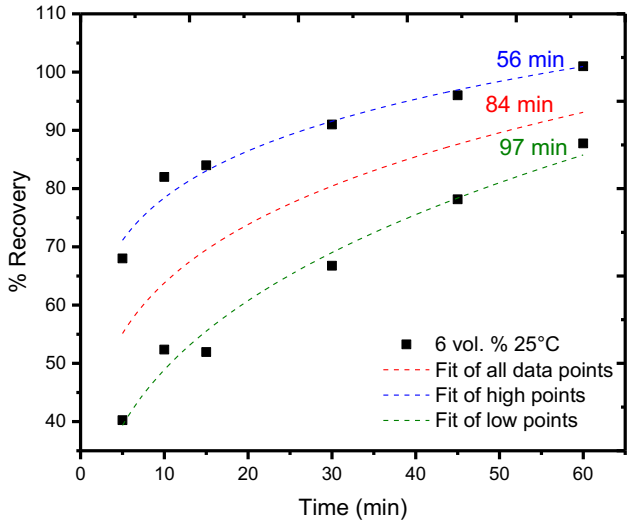

Figure S18 Recovery versus time data for 6 vol. % 25°C with power law fits of all, high, and low data points.

Table S10. Power law fits of 6 vol. % 25°C from Figure S10.

Data Type	Equation	Healing Time (min)
Overall, all data	$Y=39.26x^{0.211}$	84
High Points	$Y=56.69x^{0.141}$	56
Low Points	$Y=23.76x^{0.314}$	97

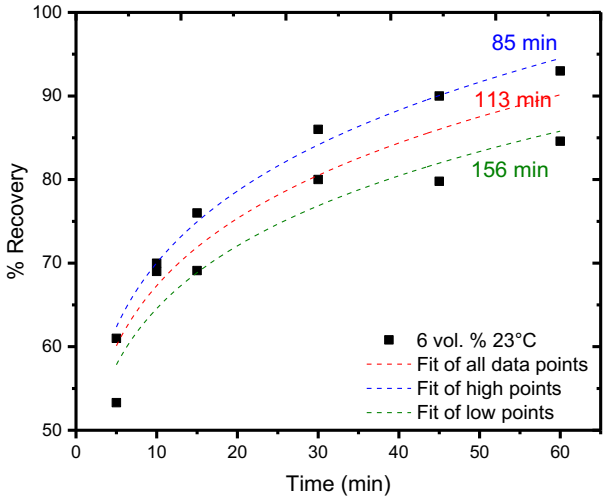

Figure S19 Recovery versus time data for 6 vol. % 23°C with power law fits of all, high, and low data points..

Table S11. Power law fits of 6 vol. % 23°C from Figure S11.

Data Type	Equation	Healing Time (min)
Overall, all data	$Y=43.22x^{0.163}$	113
High Points	$Y=47.64x^{0.167}$	85
Low Points	$Y=44.80x^{0.159}$	156

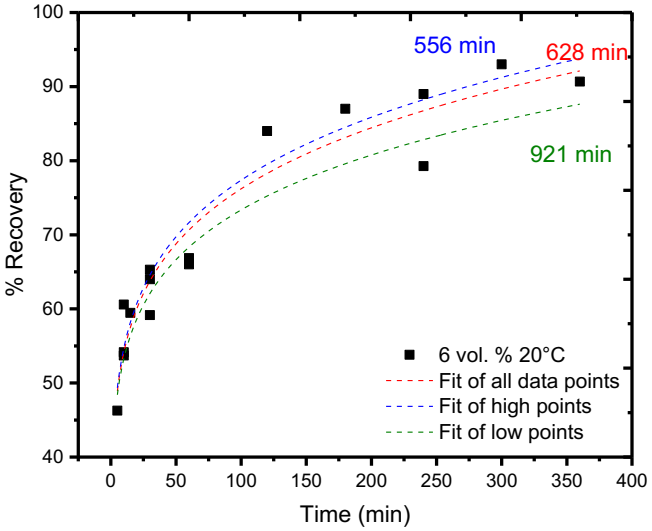

Figure S20 Recovery versus time data for 6 vol. % 20°C with power law fits of all, high, and low data points.

Table S12. Power law fits of 6 vol. % 20°C from Figure S12.

Data Type	Equation	Healing Time (min)
Overall, all data	$Y=38.54x^{0.148}$	628
High Points	$Y=38.75x^{0.150}$	556
Low Points	$Y=38.72x^{0.139}$	921